ACS OMEGA

Open Access

http://pubs.acs.org/journal/acsodf

Article

Durability of a Metakaolin-Incorporated Cement-Based Grouting Material in High Geothermal Tunnels

Lidan Fan, Guangzhi Ren, Yongqiang Yu,* Liang Sun, Peitao Li, Jiyun Zhang, and Zhouhu Su

Cite This: *ACS Omega* 2024, 9, 44251−44261

Read Online

ACCESS | Metrics & More | Article Recommendations

ABSTRACT: To improve the durability of cement-based grout in high geothermal tunnel grouting projects, metakaolin was incorporated to replace 8% of the cement. The permeability, chloride penetration, and sulfate and carbonate erosion tests were carried out on the grout cured at varying temperatures (20, 30, 40, 50, and 60 °C). It was shown that with the increase in curing temperature, the impermeability and resistance to chloride penetration initially increased and then decreased, reaching the highest values at 40 °C. Furthermore, the incorporation of metakaolin into grout enhanced the impermeability by 11.11−38.91% and resistance to chloride penetration by 12.23−12.77%. As attacked by sulfate, the surface spalling of the specimen was more obvious with the increase in the curing temperature and immersion time. Conversely, the appearance remained almost unchanged under carbonate erosion. As immersion time increased, both the antisulfate and anticarbonate erosion coefficients declined. The effect of curing temperature on erosion resistance was assessed via the relative antierosion coefficient. When immersed in sulfate, the coefficient achieved the highest value of 1.08 as cured at 30 °C, and in carbonate, the coefficient reached a maximum of 0.99 as cured at 40 °C. Through scanning electron microscopy and binarized images, it was verified that gypsum and ettringite were formed during sulfate attack, leading to volume expansion and cracking, consequently reducing the strength. Meanwhile, in the case of carbonate erosion, calcium hydroxide (CH) and calcium silicate hydrate gel (C-S-H) were dissolved and degraded, resulting in a large number and size of pores in the grout. The research results have certain theoretical significances and reference values for the application of cement-based grouting materials in high geothermal environments.

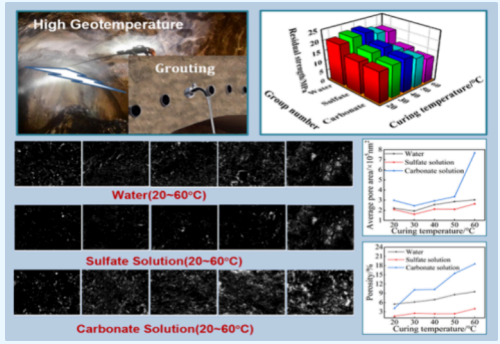

1. INTRODUCTION

With the rapid growth of the depth and scale of underground engineering such as transportation and water conservancy, a number of longer, larger, and deeper tunnels will be built in the fields of railway, highway, and hydropower, and the engineering geological environment will be more complicated. Due to the influence of geological structures, tunnel burial depth, magma, and hot groundwater activity, some regions will form high geothermal areas.[1,2] In the western part of the United States, primarily in Nevada, Idaho, and California, high geotemperatures and high heat flow are widespread located, e.g., the geotemperature is as high as 47 °C in the Tecolote Road Tunnel.[3,4] The typical temperatures of tunnel rock walls are around 40 °C in the Gotthard Base Tunnel and Lötschberg Basis Tunnel in Switzerland,[5] and the international infrastructure of the Lyon-Turin Base Tunnel, crossing the Alps and meeting uncommon conditions, reaches a peak temperature of 47 °C.[6] In China, there are 10 geothermal tunnels along the CZ Railway. More than a quarter of the Gaoligongshan Tunnel of the Dali-Ruili Railway is at risk of heat damage, with the highest geotemperature reaching 50 °C. The highest measured rock temperature in the Jiwoxiga Tunnel on the Lhasa-Shigatse Railway Line reaches 65.4 °C.[7,8]

Cement grouting is a technical method to reinforce the surrounding rock and ensure the safety of tunnel construction. However, external conditions such as high geothermal temperatures, groundwater, and erosion environments will have significant negative effects on the grout durability. CO_2 is one of the mainly present in the geothermal reservoirs, and CO_2 corrosion in the Imperial Valley of California is very common.[9] The salt of very high content was also found in areas of geothermal deep infrastructures.[10] In addition, the fluid in the geothermal environment changed due to temperature, altering its pH value, which affected fluid corrosion.[11] Therefore, corrosion in environments affected by underground hot water needs to be considered in geothermal tunnels. Under high geothermal conditions, the properties of Portland cement grout are markedly different from those of

Received: May 9, 2024
Revised: October 15, 2024
Accepted: October 18, 2024
Published: October 24, 2024

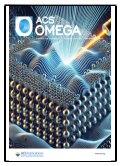

normal temperature. The high temperature led to incomplete hydration, resulting in decreased later strength and increased permeability of the cement grout, which had a detrimental impact on the durability of the grout.[12,13] Furthermore, research literature on cement grout durability indicated that Portland cement exhibited poor resistance in corrosive acidic environments.[14] Cement-based materials may soften after being eroded by external sulfate and may even flake off in severe cases. Also, the generated needle-like ettringite would lead to the volume expansion of the grout, ultimately compromising durability.[15] Chen et al.[16] evaluated the effect of sulfate attack on cement-based materials using nonlinear shock resonance acoustic spectroscopy. After 2 and 3 months of erosion, the nonlinear parameter increased by about 140 and 3700%, respectively. Other literature indicated that the essence of sulfate attack on cement-based grout is that sulfate ions react with cement hydration products, precipitating expansion products such as gypsum and ettringite, or causing the loss of cementation properties of cementitious components, which ultimately leads to cracking or strength damage of grouting stones.[14,17] The exposure of grout to a sodium carbonate environment leads to the precipitation of calcium carbonate ($CaCO_3$) inside the material. This precipitate envelops the unhydrated cement particles, affecting the degree of cement hydration. Meanwhile, this precipitate might result in deterioration of the properties and durability of cement.[18] As it was attacked by carbonate, the CH in the cement-based grout was dissolved, and the pH value of the pore solution decreased. Eventually, the cementitious components were leached, resulting in an increase in internal porosity and permeability.[19,20]

Li et al.[21] proposed a new transport model to describe chloride penetration in cement-based grouting materials and summarized the influence of pore size distribution on chloride transport. Hong et al.[22] applied nanoclay to cement slurry and found that the addition of nanoclay reduced the porosity of the stone structure, improved the compactness of the microstructure, effectively inhibited chloride erosion, and increased the strength of the stone. Wang et al.[23] found that reactive powder cement concrete was eroded by chloride salt under the action of freeze−thaw cycles. Compared with that of C50 concrete, its compressive strength exhibited a different development trend and showed good durability.

The addition of mineral admixtures with pozzolanic effects can enhance the performance of cement. Metakaolin contains high levels of active Al_2O_3 and SiO_2, enabling it to exhibit significant pozzolanic activity. The extra C-S-H gel produced by pozzolanic reactions, as well as filling behavior in later stages, densified the hardened cement paste and blocked the capillary pores' connection. Therefore, metakaolin can improve the strength, impermeability, and durability of the cement-based materials. Wang et al.[24] used ultrafine metakaolin to replace part of Portland cement and concluded that adding ultrafine metakaolin could improve the compressive strength of cement grout. Feng and Liu[25] applied the method of adding metakaolin to geopolymer cement to conduct durability tests including impermeability, antisulfate erosion, etc. It was shown that the addition of appropriate metakaolin could significantly improve the durability of the geopolymer cement.

The high temperature environment accelerated the movement of water molecules and erosive ions during the permeation process to a certain extent,[26] which was more unfavorable to the durability of cement grout under corrosive conditions. Therefore, it is necessary to pay extra attention to the durability of grouting materials in a high geothermal tunnel. However, there is currently very little research in this field. In this paper, under simulated high geothermal environments, first, the improvements in durability due to metakaolin were verified through tests on impermeability and chloride penetration. Subsequently, the grout containing metakaolin was evaluated for its antisulfate erosion and anticarbonate erosion performance. This paper provides a reference for the application of cement-based grout in high geothermal tunnel engineering.

2. RESULTS AND DISCUSSION

2.1. Impermeability. The permeability of the grout is depicted in Figure 1. It can be seen that with the increase in curing temperature, the impermeabilities of both grouts first increase and then decrease, reaching the peak at 40 °C. The proper elevation of curing temperatures was beneficial in enhancing the pozzolanic effect of metakaolin, improving the hydration degree of cement grout, compacting the internal structure, and thereby reducing its permeability. However, when the curing temperature was over 40 °C, it was easy to produce a C-S-H gel with low gel porosity. Besides, the early hydration products were rapidly produced and precipitated, the hydration products were disorderly overlapped, and the coarse porosity increased.[27] At the same time, the rapid evaporation of internal moisture also caused more pores inside the specimen, leading to an increase in the permeability. Compared with the standard curing temperature, the permeability of specimens containing metakaolin decreased by 80.8, 93.15, and 54.11 and increased by 80.82% at curing temperatures of 30, 40, 50, and 60 °C, respectively. It can be concluded that an appropriately elevated curing temperature played a positive role in enhancing the impermeability of the grout and there was a temperature threshold.

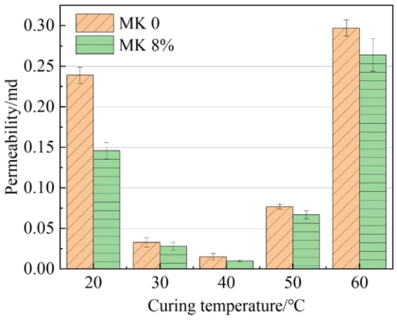

Figure 1. Permeability of grout cured at different temperatures.

Additionally, at each curing temperature, the permeability of the metakaolin-incorporated cement-based grout (MPC) was reduced by 38.91, 15.15, 33.33, 12.99, and 11.11% in comparison to that of ordinary Portland cement grout (OPC), respectively. It is attributed to the refinement of internal pores in the grout through the pozzolanic reaction of metakaolin. Moreover, since the particles of metakaolin are smaller than those of cement (see Figure 19), the unreacted metakaolin can play a filling role in the micropores, leading to the denser grout.

2.2. Resistance to Chloride Penetration. The electric flux of the grout is depicted in Figure 2. As the curing temperature increased, the electric flux of MPC and OPC

https://doi.org/10.1021/acsomega.4c04434
ACS Omega 2024, 9, 44251−44261

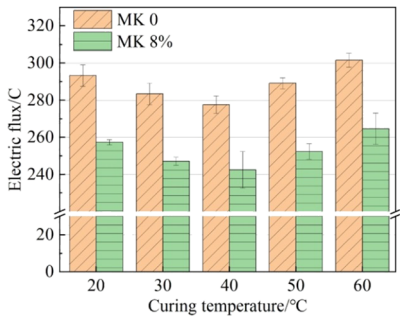

Figure 2. Electric flux of grout cured at different temperatures.

grouts initially decreased and then increased. This indicates that the resistance to chloride penetration initially increased and then decreased, reaching its optimum value when the grout was cured at 40 °C.

The electric flux of MPC decreased by 12.24, 12.77, 12.64, 12.73, and 12.23%, respectively, compared with that of the OPC when cured at temperatures of 20, 30, 40, 50, and 60 °C. On the one hand, the increased compactness is attributed to metakaolin's pozzolanic; on the other hand, it is due to the grout containing metakaolin having a higher chloride combining ability and the aluminate inside metakaolin combining with chloride to form Friedel's salt, which delays the penetration of chloride. Additionally, metakaolin, possessing a high content of aluminum, could facilitate the formation of additional AFM phases, which further influenced chloride penetration.[28]

The effect of the temperature on the resistance to chloride penetration is similar to its effect on impermeability. The relationship curve between electric flux and permeability is depicted in Figure 3, showing a positive correlation. That is, as

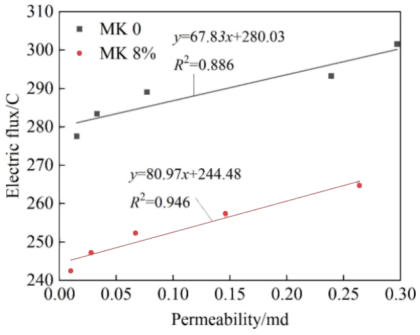

Figure 3. Relationship between electric flux and permeability.

the permeability of the grout increased, the diffusion rate of chloride was affected and the electric flux also increased. Metakaolin had a certain reduction effect on both the impermeability and resistance to chloride penetration. However, from the slopes of the two fitting lines, it can be inferred that the effect of metakaolin on the interaction between them remained largely unchanged.

Based on the above results and discussion, it was concluded that the addition of metakaolin contributed to improving the waterproofing and resistance to chloride penetration of the grout. The erosion of MPC in sulfate and carbonate solutions will be investigated in the next two sections. The reduction in compressive strength of the grout under acid exposure was a key factor; therefore, the residual compressive strength was used to illustrate the erosion characteristics.

2.3. Performance of Antisulfate Erosion. *2.3.1. Visual Inspection.* Figure 4a,c presents the specimens immersed in water, while Figure 4b,d presents the specimens immersed in Na_2SO_4 solution. It can be observed that sulfate erosion caused the surfaces of specimens to peel off, and edge degradation was obvious, which was also mentioned in the literature.[29] In the same immersion time *t*, specimens cured at different temperatures showed various degrees of deterioration in Na_2SO_4 solution, with the degree positively correlated with the curing temperature. At the same curing temperature, with the increase in immersion time *t*, the degradation also appeared in specimens cured at lower temperatures. Furthermore, Figure 4d shows that the remarkable deterioration occurred after immersion in sulfate solution for 60 days for the specimen cured at 60 °C, presenting a nonprismatic characteristic.

2.3.2. Compressive Strength Loss. The compressive strength variation of the specimens immersed in a sulfate solution is exhibited in Figure 5. In Figure 5a, the initial compressive strength, i.e., specimens immersed for 0 days, first increases and then decreases, reaching its maximum value at 40 °C, which is consistent with the phenomena impermeability and resistance to chloride penetration.

When immersed in water, the compressive strength of the specimens immersed for 30 days was lower than that for 0 days. When the specimens were placed in water, the hydration product CH would be dissolved and the C-S-H gel might decompose subsequently, resulting in a decline of the compressive strength. More importantly, the hydration reaction of incompletely hydrated cement would continue, bringing about a denser structure than before,[30] and lead to an improvement in compressive strength. It should be noted the compressive strengths after 60 days of immersion even exceeded their initial strengths for specimens cured at 20, 50, and 60 °C, on account of the lower hydration rate at the initial stage.

In Figure 5b, the compressive strengths of the specimens cured at 20, 30, and 40 °C reach their maximum values after immersion for 30 days, subsequently decreasing to values lower than the initial. Also, the compressive strength of the specimens cured at 50 and 60 °C keep dropping with the increase in immersion time. In addition, the residual compressive strengths exposed to sulfate solution were much lower than those in water after the same immersion time.

The sulfate erosion process is mainly associated with the products of dihydrate gypsum ($Ca_2SO_4{\cdot}2H_2O$) and ettringite ($Ca_6Al_2(SO_4)_3(OH)_{12}{\cdot}26H_2O$), and it can be divided into two processes, namely, filling and expansion cracking. With the increase in immersion time *t*, SO_4^{2-} intruded into the grout and reacted with CH and C-S-H to form dihydrate gypsum and ettringite, as shown in eqs 1 and 2, respectively

$$Ca(OH)_2 + SO_4^{2-} + 2H_2O \rightarrow Ca_2SO_4{\cdot}2H_2O + 2OH^- \quad (1)$$

$$Ca_3Al_2O_6{\cdot}6H_2O + 3(CaSO_4{\cdot}2H_2O) + 20H_2O \rightarrow Ca_6Al_2(SO_4)_3(OH)_{12}{\cdot}26H_2O \quad (2)$$

These reaction products would fill the internal pores of the specimen without expansion in the early stage of immersion,[31] so enhanced compressive strength was presented. When the

https://doi.org/10.1021/acsomega.4c04434
ACS Omega 2024, 9, 44251−44261

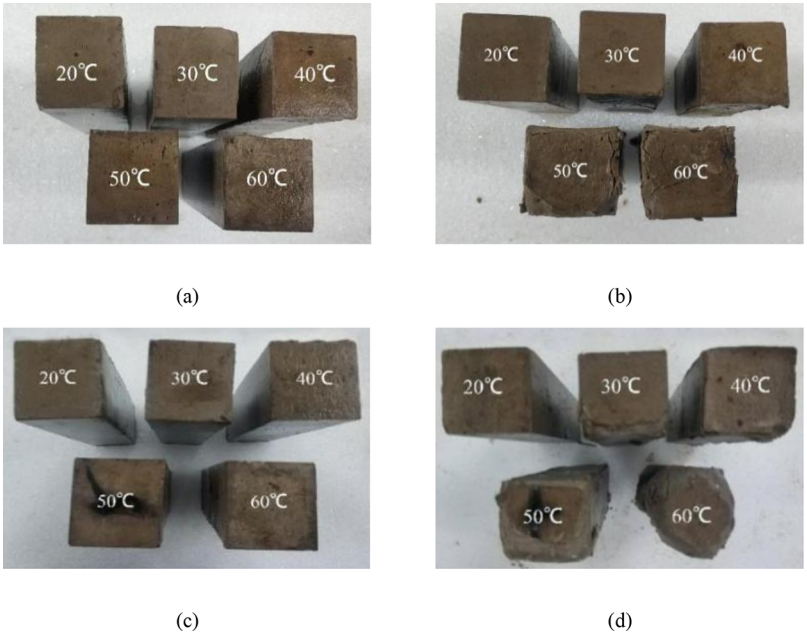

Figure 4. Photograph of specimens immersed in water and sulfate solution: (a) water for 30 days; (b) sulfate for 30 days; (c) water for 60 days; and (d) sulfate for 60 days.

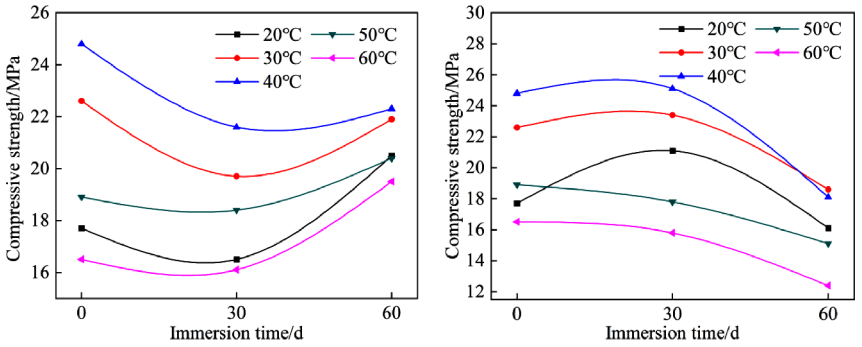

Figure 5. Variation of the specimen compressive strength with immersion time: (a) water and (b) sulfate solution.

internal pores were filled, the reactions shown in eqs 1 and 2 continued. The subsequent generated ettringite adhered to the previously ettringite and continued to grow, as well as the volume expanded resulting from the generation of dihydrate gypsum and some sulfate crystals. The stress induced by expansion and crystallization pressure inside the grout, leading subsequently to the spalling and cracking, which gradually resulted in the destruction of the grout. Additionally, with the decrease in the pH of the cementitious material on account of the consumption of CH, decalcification of the C-S-H gel might take place, which also was detrimental to the grout.

The above process had a great dependence on the porosity inside the grout, which was closely related to the curing temperature. For the grout cured at temperatures not exceeding 40 °C, the erosion process involved two processes: filling and expansion cracking. However, for the grout cured at 50 and 60 °C, due to the more and coarser internal pores, the sulfate diffusion and the reaction rate with CH and C-S-H were accelerated. Consequently, the grout entered the expansion cracking stage prior to the 30 day immersion period, resulting in a decline in strength at that moment. This phenomenon corresponds to the observed sulfate erosion of the grout, mentioned above.

2.3.3. Antisulfate Erosion Coefficient and Relative Antisulfate Erosion Coefficient. The $K_{sulfate}$ of the grout was calculated according to eq 7, as shown in Figure 6. It decreased with immersion time t from 30 to 60 days. When t was 30 days, the $K_{sulfate}$ of the grouts cured at 20, 30, and 40 °C were greater

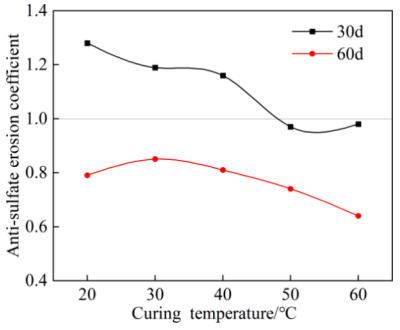

Figure 6. Antisulfate erosion coefficient.

https://doi.org/10.1021/acsomega.4c04434
ACS Omega 2024, 9, 44251−44261

than 1.0, while those for grouts cured at 50 and 60 °C were less than 1.0, indicating reduced erosion resistance with the increase in curing temperature. After 60 days of exposure, all of the $K_{sulfate}$ values were less than 1.0, with the largest value observed at 30 °C, indicating that it possessed the best resistance to erosion.

The $K_{r\text{-}sulfate}$ of the grout was determined by using eq 8, as depicted in Figure 7. With the increase in immersion time t,

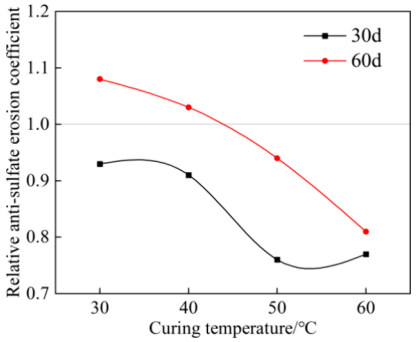

Figure 7. Relative antisulfate erosion coefficient.

the $K_{r\text{-}sulfate}$ increased. At 30 days, the $K_{r\text{-}sulfate}$ of grout at each curing temperature was less than 1.0 and decreased with the increase in curing temperature. This indicates that the elevating of curing temperature has a negative effect on the sulfate resistance of grout in the short-term erosion. At 60 days, the $K_{r\text{-}sulfate}$ of grouts cured at 30 and 40 °C were greater than 1.0, suggesting that moderately raising the curing temperature positively affects resistance to long-term sulfate attack. Furthermore, the grout cured at 30 °C exhibited the optimal performance of antisulfate erosion.

2.4. Performance of Anticarbonate Erosion. *2.4.1. Visual Inspection.* The specimens after immersion in the carbonate solution for 60 days are depicted in Figure 8. In

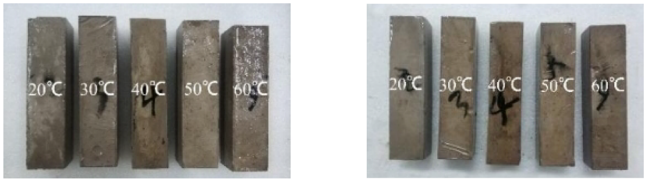

(a) (b)

Figure 8. Photograph of specimens immersed in carbonate solution: (a) for 30 days and (b) for 60 days.

comparison with the specimens immersed in sulfate solution, no obvious spalling or cracking was observed, which indicates that the erosion mechanism differs from that of sulfate erosion.

2.4.2. Compressive Strength Loss. The variation of the compressive strength with the time of carbonate erosion is depicted in Figure 9. The grout with higher initial compressive strength retained a correspondingly higher residual compressive strength, showing good consistency between the two. The compressive strength increased by 2−13% for different curing temperatures at t of 30 days and then decreased to 70−80% of the initial compressive strength as immersed to 60 days.

When the grout specimens were immersed in carbonate solution, the erosion process mainly includes three stages: carbonization, dissolution, and C-S-H gel decalcification. In the

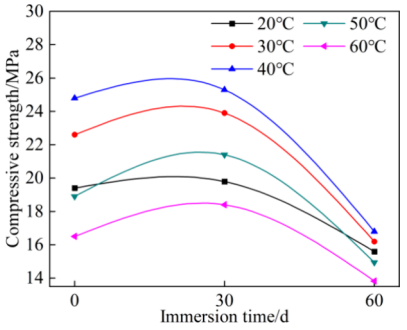

Figure 9. Variation of the specimen compressive strength with immersion time in carbonate solution.

initial stage, CO_3^{2-} enters the interior of the grout and reacts with the hydration product CH to form $CaCO_3$, as shown in eq 3

$$Ca(OH)_2 + CO_3^{2-} \rightarrow CaCO_3 + 2OH^- \quad (3)$$

The generated $CaCO_3$ fills the internal pores. This process reduces internal porosity and pore size, thereby increasing the compressive strength. Furthermore, the corrosion product $CaCO_3$ reacts with carbonic acid to form $Ca(HCO_3)_2$, as shown in eq 4

$$CaCO_3 + CO_3^{2-} + 2H^+ \rightarrow Ca(HCO_3)_2 \quad (4)$$

The product of $Ca(HCO_3)_2$ is soluble in water and continuously leaches out, resulting in a decrease in the CH concentration in the grout. Since then, the acidification of the grout may also lead to the decalcification of the C-S-H gel, as shown in 5

$$\text{C-S-H} + CO_3^{2-} \rightarrow CaCO_3 + \text{Ca} - \text{depleted C-S-H} \quad (5)$$

The decalcification of the C-S-H gel will lead to the destruction of the internal microstructure and a decline of the compressive strength. Thus, the CH content is the primary factor affecting carbonate erosion, with the effect of porosity being lower than that of the CH content.[19] After long-term erosion of carbonate, the compressive strength of the grout decreased significantly, whereas the appearance did not change significantly. The main mechanism of carbonate erosion involves the dissolution of hydration products in the hardened grout, which differs from the expansion and cracking damage caused by sulfate erosion. Therefore, more attention should be paid to carbonate erosion in engineering.

2.4.3. Anticarbonate Erosion Coefficient and Relative Anticarbonate Erosion Coefficient. The $K_{carbonate}$ is depicted in Figure 10. With the extension of immersion time t from 30 to 60 days, the $K_{carbonate}$ of grouts at different curing temperatures decreased. When immersed for 30 days, the $K_{carbonate}$ was greater than 1.0. However, it decreased slightly with the increase in curing temperature. After immersion for 60 days, the $K_{carbonate}$ fluctuated around 0.73, indicating that the curing temperature had little effect on the resistance to long-term carbonate attack.

In Figure 11, the $K_{r\text{-}carbonate}$ increased with the extension of the erosion time. When t was 30 days, it decreased with the increase in curing temperature; nevertheless, it remained above 0.85. When t was 60 days, it initially increased and then decreased as the curing temperature increased, remaining above 0.90. These results indicate that under carbonate

https://doi.org/10.1021/acsomega.4c04434
ACS Omega 2024, 9, 44251−44261

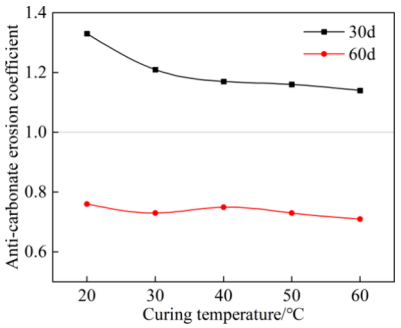

Figure 10. Anticarbonate erosion coefficient.

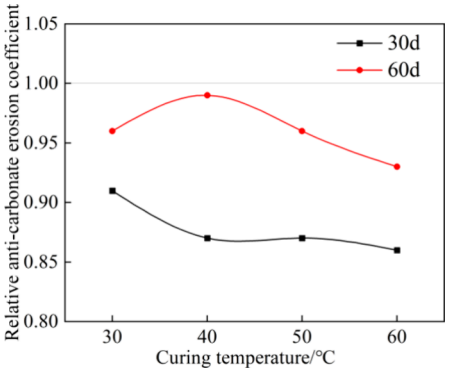

Figure 11. Relative anticarbonate erosion coefficient.

erosion, higher curing temperatures initially have some adverse effects on carbonate resistance, but this effect diminishes with prolonged erosion time.

2.5. Microstructural Analysis. *2.5.1. Micromorphology of Eroded Grout.* Figures 12, 13, and 14 are the SEM images (×5000) of MPC after immersion in water, sulfate solution, and carbonate solution for 60 days, respectively. It can be observed from Figure 12 that the specimens generally exhibited a denser microstructure as the hydration reaction continued and additional hydration products were produced during immersion in water. However, there were varying levels of density among the specimens cured at different curing temperatures. It presents a particularly porous structure for the specimen cured at 60 °C, as shown in Figure 12e. In Figure 13, a certain amount of ettringite formed after exposure to sulfate, with some disordered columnar gypsum present inside, consistent with the specimen's morphology. Because the C-S-H gel was decalcified and decomposed, the structure became loose, which matched very well with the compressive strength, especially for specimens cured at 60 °C in Figure 13e. Figure 14 depicts an undense C-S-H gel in specimens exposed to carbonate. As CH dissolved, the densely arranged C-S-H gel disappeared and was replaced by an irregularly clustered C-S-H gel. This porous microstructure detrimentally affected the strength, correlating with the observed reduction in compressive strength.

Although the apparent damage to the specimen exposed to sulfate was more severe and the microstructure also changed significantly, the compressive strengths of the specimens except for those cured at 60 °C were greater than those exposed to carbonate. The pore size and porosity of the specimen cured at 60 °C were larger, which were more conducive to the entry of corrosive media. Therefore, the residual compressive strength was the lowest, and the erosion resistance was the worst.

2.5.2. Quantitative Analysis of the Microstructure of Eroded Grout. Image-Pro Plus 6.0 software was used to binarize the SEM images, as shown in Figures 15, 16, and 17. Based on the binary images, the average pore area and porosity were quantified, as shown in Figure 18. After exposure to the

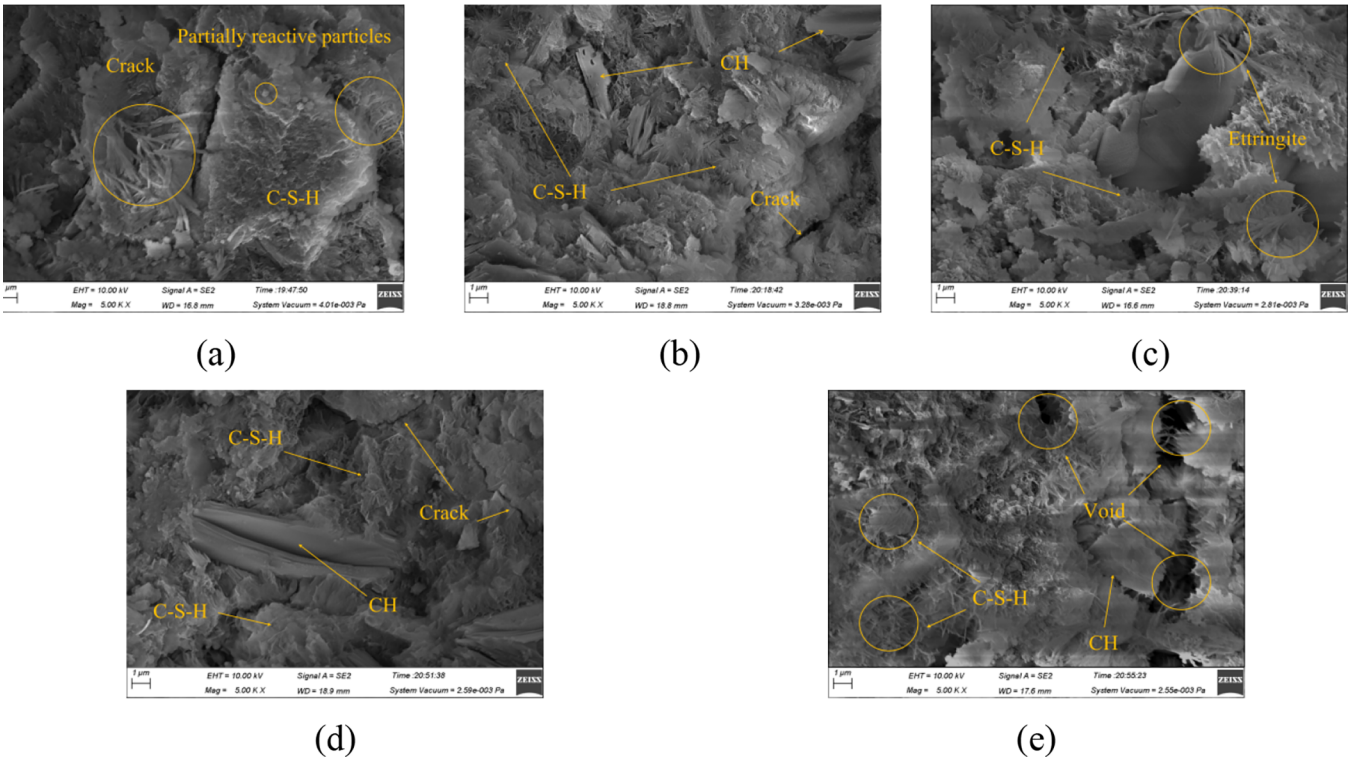

Figure 12. SEM images of specimens immersed in water: (a) 20 °C; (b) 30 °C; (c) 40 °C; (d) 50 °C; and (e) 60 °C.

https://doi.org/10.1021/acsomega.4c04434
ACS Omega 2024, 9, 44251−44261

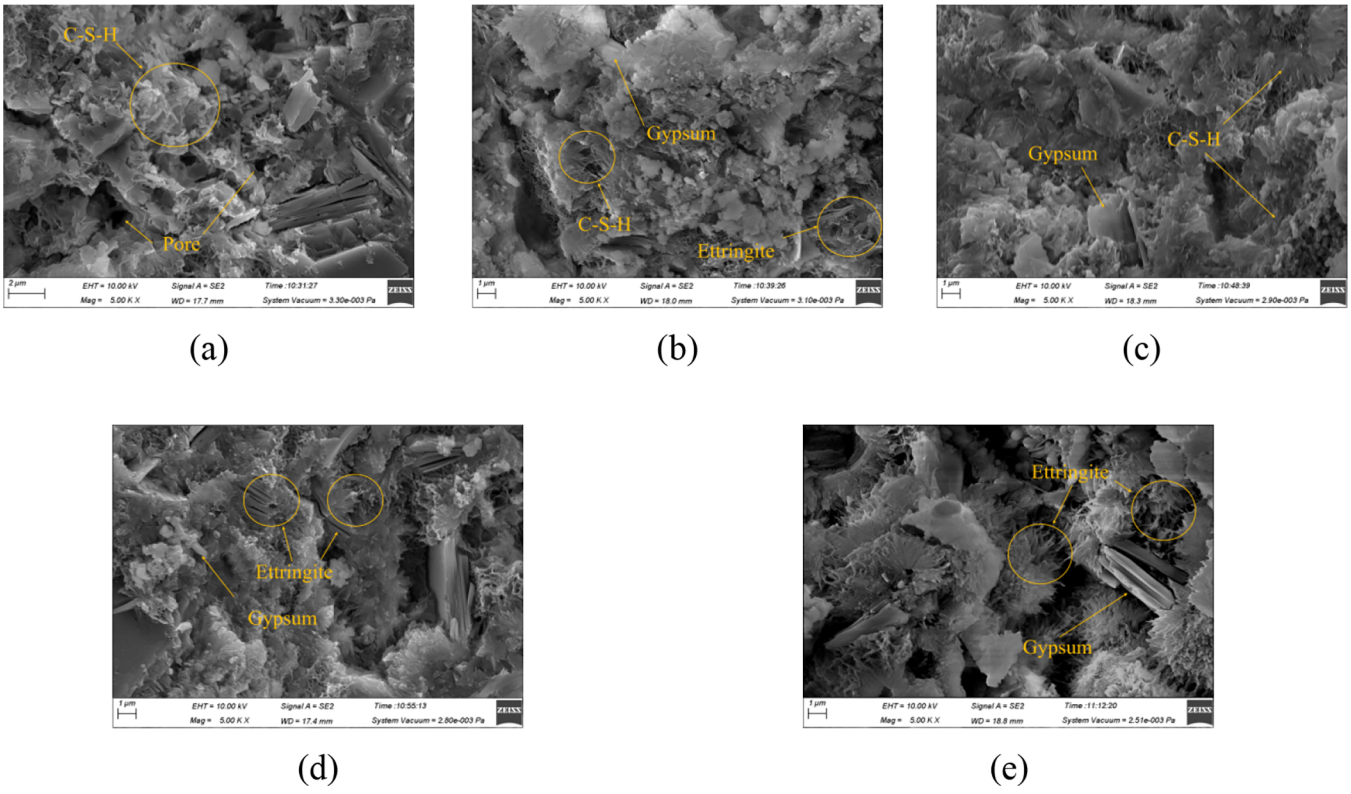

Figure 13. SEM images of specimens immersed in sulfate solution: (a) 20 °C; (b) 30 °C; (c) 40 °C; (d) 50 °C; and (e) 60 °C.

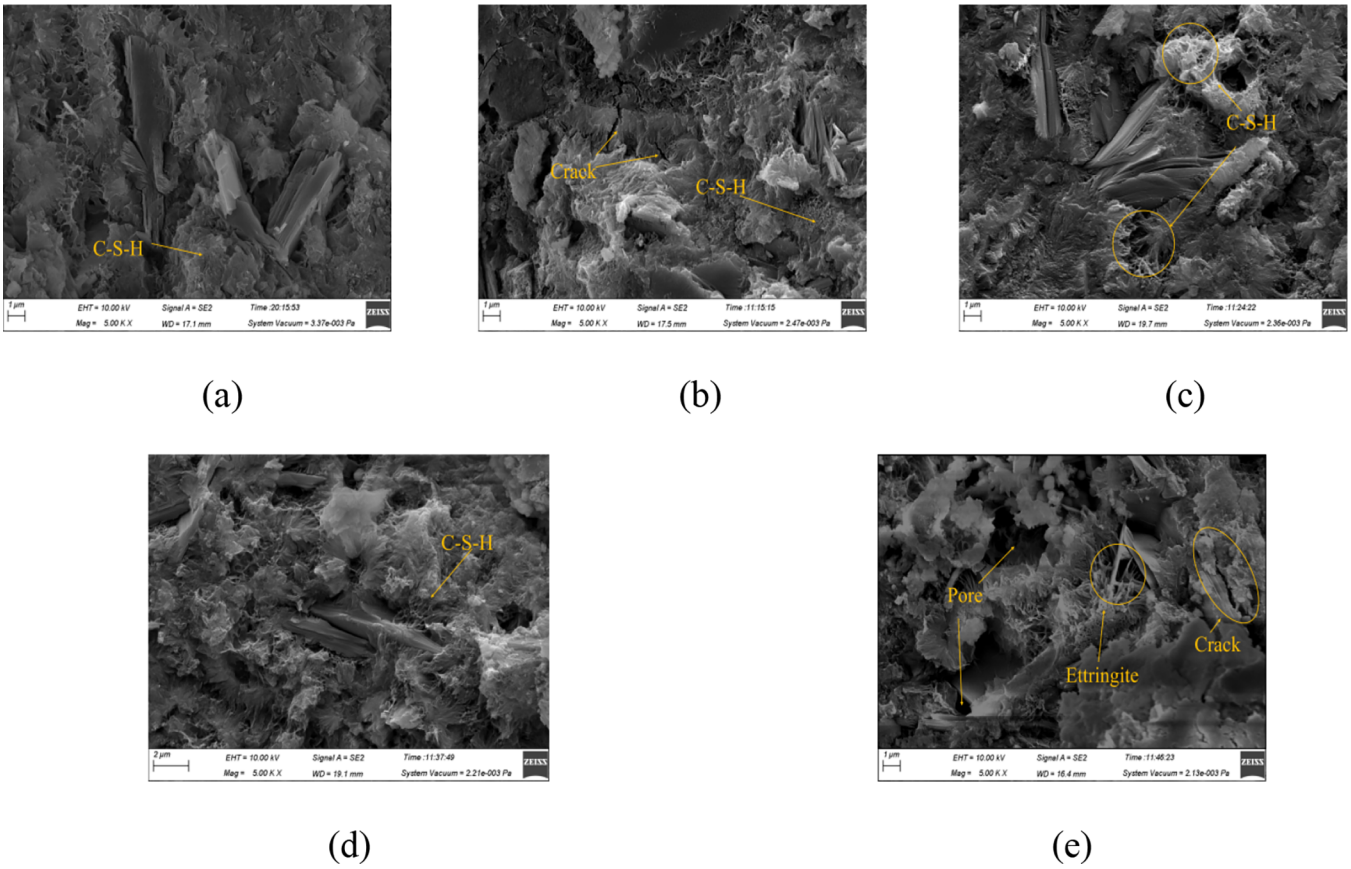

Figure 14. SEM images of specimens immersed in carbonate solution: (a) 20 °C; (b) 30 °C; (c) 40 °C; (d) 50 °C; and (e) 60 °C.

https://doi.org/10.1021/acsomega.4c04434
ACS Omega 2024, 9, 44251−44261

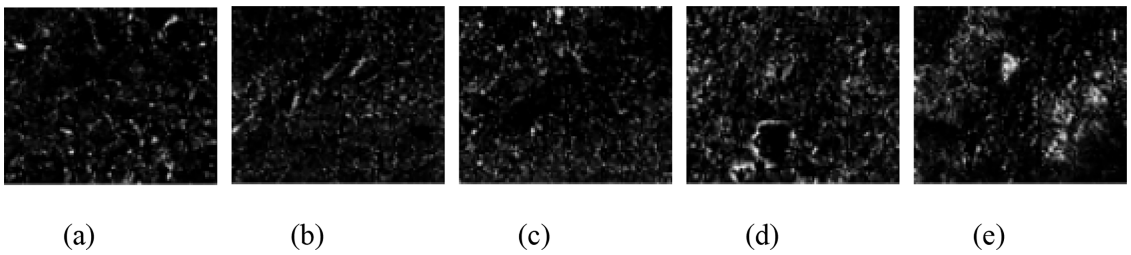

Figure 15. Binarized images of specimens immersed in water: (a) 20 °C; (b) 30 °C; (c) 40 °C; (d) 50 °C; and (e) 60 °C.

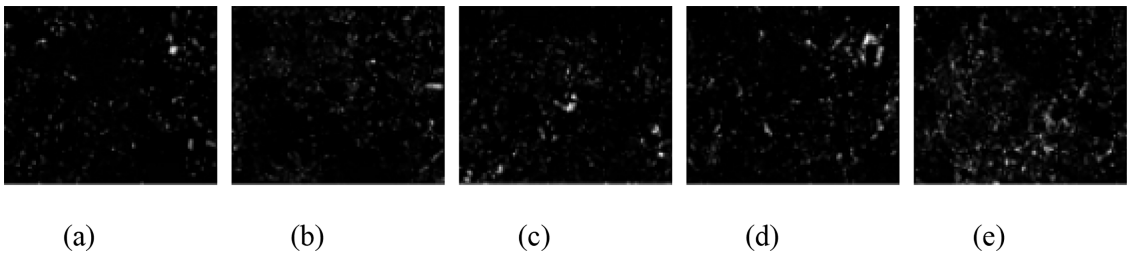

Figure 16. Binarized images of specimens immersed in sulfate solution: (a) 20 °C; (b) 30 °C; (c) 40 °C; (d) 50 °C; and (e) 60 °C.

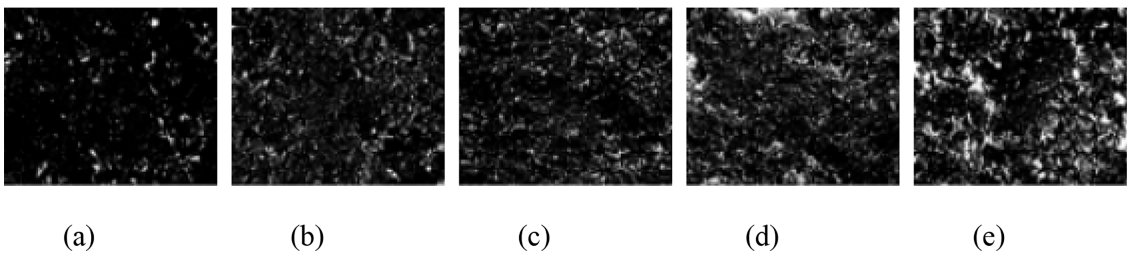

Figure 17. Binarized images of specimens immersed in carbonate solution: (a) 20 °C; (b) 30 °C; (c) 40 °C; (d) 50 °C; and (e) 60 °C.

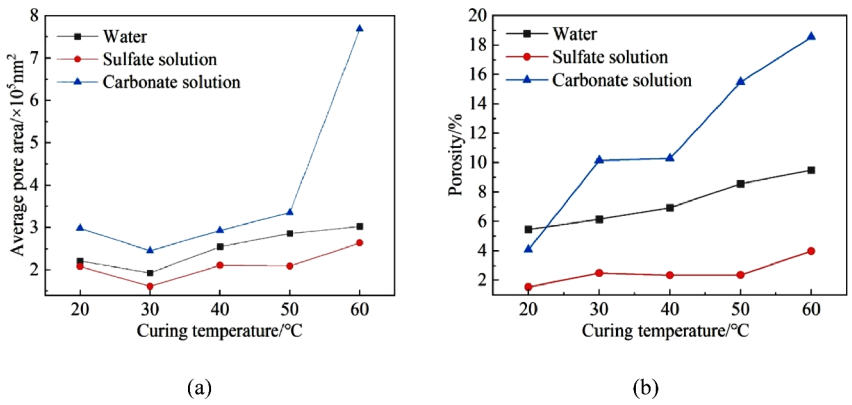

Figure 18. Pore characteristic of specimen after immersion: (a) average pore area and (b) porosity.

three media, the average pore area reached its minimum at a curing temperature of 30 °C and its maximum at 60 °C. This trend was consistent with the increase in the uneven distribution of hydration products as curing temperatures increased.

In comparison with the specimen cured at 20 °C, the porosity of grout cured at elevated temperatures increased mostly when exposed to carbonate and the least when exposed to sulfate. Thus, elevating the curing temperature would adversely affect the corrosion resistance of the grout.

The macromechanical performance of the grout was not only related to the porosity but also closely related to the pore size,[32] just like the specimens cured at 30 and 40 °C that exhibited relatively good erosion resistance as the average pore areas were smaller. There was no strictly negative linear relationship between porosity and strength, but it still showed a trend of increasing porosity with the increase in temperatures.

It was also observed that the porosity of the specimen exposed to sulfate was the smallest, being less than 4%, whereas the porosity of the specimen immersed in water was between 5 and 10%. The porosity of the specimen exposed to carbonate was the largest; except for those cured at 20 °C, all were above 10%, with the maximum reaching 18.55%. The significant difference in porosity was attributed to erosion mechanisms. Sulfate attack was mainly caused by the

https://doi.org/10.1021/acsomega.4c04434
ACS Omega 2024, 9, 44251−44261

Table 1. Main Physical Properties of Cement

parameters	fineness (m^2/kg)	initial setting time (min)	final setting time (min)	SO_3 (%)	MgO (%)	Cl^- (%)	flexural strength (MPa, 28 days)	compressive strength (MPa, 28 days)
P.O 42.5	374	166	217	2.60	4.14	0.03	8.6	48.8

Table 2. Chemical Composition of Metakaolin

composition	SiO_2	Al_2O_3	Fe_2O_3	CaO	K_2O	MgO	Na_2O	loss on ignition
content/%	54.06	43.12	0.76	0.17	0.55	0.14	0.03	1.10

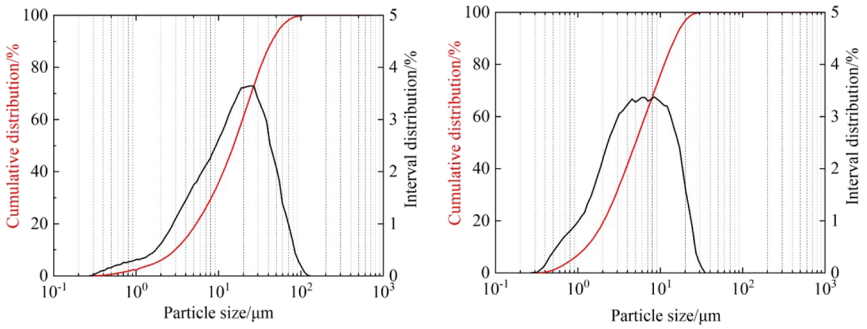

(a) Cement (b) Metakaolin

Figure 19. Particle size distribution of cement and metakaolin: (a) cement and (b) metakaolin.

crystallization stress and volume expansion of erosive products, while carbonate attack mainly involved the dissolution and degradation of hydration products.

3. CONCLUSIONS

In this article, the durability of MPC and OPC grouts cured in a simulated high geothermal environment was investigated. It is feasible to apply metakaolin to improve the durability of grout for projects in high geothermal tunnels, and the effect of the temperature on the grout resistance to erosion can be used as a reference for engineering practice. The specific conclusions are as follows:

- With the increase in curing temperature, the impermeability and resistance to chloride penetration of the grout initially increased and then decreased, reaching the peak at 40 °C. The electric flux was positively correlated with permeability. At the curing temperature of 20−60 °C, the addition of metakaolin reduced the permeability by 11.1−38.91% and the electric flux by 12.23−12.77%.
- The exposure to sulfate dramatically affected the macroscopic morphology of the specimens. The higher the curing temperature or the longer the erosion time, the more severe the degradation of the macroscopic morphology of the specimens. The specimens cured at 60 °C exhibited nonprismatic characteristics after immersion for 60 days. The exposure to carbonate erosion did not bring about obvious impact on the macroscopic morphology of the specimens.
- When exposed to sulfate for 30 days, the $K_{sulfate}$ of the grouts cured at temperatures below 40 °C were greater than 1.0, resulting from the filling of erosion products. When immersed for 60 days, the $K_{sulfate}$ were all less than 1.0, with a maximum of 0.79 and a minimum of 0.64 for 30 and 60 °C curing temperatures, respectively. The $K_{r\text{-}sulfate}$ indicated that curing at 30 and 40 °C had a positive effect on resistance to long-term sulfate attack. When exposed to carbonate for 30 days, the $K_{carbonate}$ were all greater than 1.0. After immersion for 60 days, it fluctuated around 0.73. The results of the $K_{r\text{-}carbonate}$ suggested that the elevated curing temperature had little effect on the resistance to long-term carbonate attack.
- The quantitative characterization of the microstructure of the grout was achieved by binarizing SEM images. It was further verified that the mechanism of sulfate attack was mainly the formation of gypsum and ettringite. The crystallization pressure and the volume expansion of the erosion products destroyed the specimen. The grout eroded by carbonate was mainly related to the dissolution of CH and decalcification of C-S-H, and a large number of pores, large in size, were generated inside the specimen. The specimens cured at 30 and 40 °C possessed low porosity and especially small average pore area, and it agreed well with the relatively high residual strength.

The metakaolin-incorporated cement-based grout is improved in durability compared with cement grout, and its longer-term durability could be evaluated by extending the erosion time. In addition, the coupling erosion of sulfate and carbonate in the water environment, that is, the thaumasite form of sulfate attack (TSA), is very worthy of further research.

4. MATERIALS AND METHODS

4.1. Materials. The 42.5 ordinary Portland cement (P.O. 42.5) was produced by Jiaozuo Jiangu Cement Company, with its main physical property shown in Table 1. Metakaolin was purchased from Henan Jin 'ao Refractory Materials Co., Ltd., and the chemical composition is shown in Table 2. The particle size distributions of cement and metakaolin are listed in Figure 19.

4.2. Experimental Procedure. *4.2.1. Specimen Preparation.* Two types of grouts, OPC and MPC (with 8 wt% cement replaced by metakaolin), were prepared, both of which applied the water−binder ratio of 0.8. Initially, the mixed grout was poured into the prepared test mold, and then, the poured

https://doi.org/10.1021/acsomega.4c04434
ACS Omega 2024, 9, 44251−44261

specimen was placed at the specific temperature (20, 30, 40, 50, and 60 °C, 20 °C as the control group, RH ≥ 90% in the curing box) for steam curing. After curing for 24 h, the specimen was disassembled and then placed on the bracket in the corresponding environment to continue curing until 28 days. The specimens, cured to the specified age, were used to conduct various durability tests.

4.2.2. Test Methods. 4.2.2.1. Impermeability. A TC-III multilayer superimposed gas reservoir joint development simulator was utilized to investigate the grout impermeability, with the permeability of the 40 mm × 40 mm × 160 mm specimen applied as the impermeability indicator. The principle of the permeability test is based on the Darcy flow model. The average permeability K is calculated based on parameters that include the nitrogen flow through the specimen and the pressure difference between its inlet and outlet, as shown in eq 6

$$k = \frac{2\mu L Q_0 P_0 \times 100}{(P_1^2 - P_2^2)S} \tag{6}$$

where k is the gas permeability ($10^{-3}\mu m^2$), μ is the dynamic viscosity of nitrogen at 25 °C (mPa·s), L is the length of the specimen (cm), Q_0 is the seepage flow under standard atmospheric pressure (cm^3/s), P_0 is the standard atmospheric pressure (MPa), P_1 is the inlet gas pressure (MPa), P_2 is the outlet gas pressure (MPa), and S is the cross-sectional area of the specimen (cm^2).

4.2.2.2. Resistance to Chloride Penetration. The resistance of the grout to chloride penetration was tested by the electric flux method in ASTM C1202. Cylindrical specimens with diameters of 100 mm and heights of 50 mm were used for testing.

4.2.2.3. Erosion Resistance. The specimens, cured for 28 days, were immersed in water, 5% Na_2SO_4 solution, and 5% Na_2CO_3 solution. The immersion time (t) was 0, 30, or 60 days. During the immersion period, the solutions were replaced biweekly until the end of the immersion period. After immersion, the residual compressive strength was tested, and the antierosion coefficient K_{medium} (including $K_{sulfate}$ and $K_{carbonate}$) was defined as the evaluation indicator of erosion, as shown in eq 7

$$K_{medium} = \frac{f_{medium}}{f_{water}} \tag{7}$$

where K_{medium} is the antierosion coefficient, f_{medium} is the residual compressive strength of the specimen after immersion time (t) in the erosion solution (MPa), and f_{water} is the compressive strength of the specimen after immersion time (t) in water (MPa).

The effect of elevated curing temperatures on the resistance to erosion was investigated, with a curing condition of 20 °C as the control group. The relative antierosion coefficient is defined according to eq 8

$$K_{r\text{-}medium,T} = \frac{K_{medium,T}}{K_{water,20°C}} \tag{8}$$

where $K_{r\text{-}medium,T}$ is the relative antierosion coefficient of the specimen cured at T temperature, $K_{medium,T}$ is the antierosion coefficient of the specimen cured at T, and $K_{medium,20°C}$ is the antierosion coefficient of the specimen cured at 20 °C.

AUTHOR INFORMATION

Corresponding Author

Yongqiang Yu − *School of Civil Engineering and International Joint Research Laboratory of Henan Province for Underground Space Development and Disaster Prevention, Henan Polytechnic University, Jiaozuo, Henan 454000, China*; Email: yyq@hpu.edu.cn

Authors

Lidan Fan − *School of Civil Engineering and International Joint Research Laboratory of Henan Province for Underground Space Development and Disaster Prevention, Henan Polytechnic University, Jiaozuo, Henan 454000, China*; orcid.org/0000-0002-6025-3769

Guangzhi Ren − *School of Civil Engineering, Henan Polytechnic University, Jiaozuo, Henan 454000, China*

Liang Sun − *China Construction Fifth Engineering Bureau Co., Ltd., Changsha, Hunan 410004, China*

Peitao Li − *School of Civil Engineering, Henan Polytechnic University, Jiaozuo, Henan 454000, China*

Jiyun Zhang − *School of Civil Engineering, Henan Polytechnic University, Jiaozuo, Henan 454000, China*

Zhouhu Su − *School of Civil Engineering, Henan Polytechnic University, Jiaozuo, Henan 454000, China*

Complete contact information is available at: https://pubs.acs.org/10.1021/acsomega.4c04434

Notes

The authors declare no competing financial interest.

ACKNOWLEDGMENTS

This research work was funded by the National Natural Science Foundation of China Youth Fund Project (52208244), Scientific and Technological Research Projects in Henan Province (222102320034), and Cultivation Project of National Natural Science Foundation of China for Double First-Class Discipline Construction in Henan Polytechnic University (AQ20240730). The authors are also very grateful to editors and reviewers for their work.

REFERENCES

(1) Yunpeng, H.; Mingnian, W.; Zhilong, W.; Qiling, W.; Dagang, L. Mechanical behavior and constitutive model of shotcrete-rock interface subjected to heat damage and variable temperature curing conditions. *Constr. Build. Mater.* **2020**, *263*, No. 120171.

(2) Duan, L.; Zhang, Y.; Lai, J. Influence of ground temperature on shotcrete-to-rock adhesion in tunnels. *Adv. Mater. Sci. Eng.* **2019**, *2019*, 8709087.

(3) Swanberg, C. A.; Morgan, P. The linear relation between temperatures based on the silica content of groundwater and regional heat flow: a new heat flow map of the United States. *Pure Appl. Geophys.* **1978**, *117*, 227−241.

(4) Zhang, G.-Z.; Cao, Z.-M.; Xiao, S.-G.; Guo, Y.-M.; Li, C.-l. A promising technology of cold energy storage using phase change materials to cool tunnels with geothermal hazards. *Renew. Sust. Energy. Rev.* **2022**, *163*, No. 112509.

(5) Wilhelm, J.; Rybach, L. The geothermal potential of Swiss Alpine tunnels. *Geothermics.* **2003**, *32*, 557−568.

(6) Alvi, M. R.; Insana, A.; Barla, M. Thermal performance assessment of an energy lining for the Lyon-Turin base tunnel. *Soils Rocks* **2022**, *45*, No. e2022000722.

(7) Zhang, D.; Sun, Z.; Fang, Q. Scientific problems and research proposals for Sichuan−Tibet railway tunnel construction. *Undergr. Space.* **2022**, *7*, 419−439.

(8) Hu, Y.-P.; Wang, Q.-L.; Wang, M.-N.; Liu, D.-G. A study on the thermo-mechanical properties of shotcrete structure in a tunnel, excavated in granite at nearly 90 °C temperature. *Tunn. Undergr. Sp. Tech.* **2021**, *110*, No. 103830.
(9) Allahvirdizadeh, P. A review on geothermal wells: Well integrity issues. *J. Clean. Prod.* **2020**, *275*, No. 124009.
(10) Baessler, R.; Burkert, A.; Saadat, A.; Kirchheiner, R.; Finke, M.Evaluation of corrosion resistance of materials for geothermal applications. *NACE Corrosion*; NACE 2009.
(11) Nogara, J.; Zarrouk, S.-J. Corrosion in geothermal environment: Part 1: Fluids and their impact. *Renew. Sust. Energ. Rev.* **2018**, *82*, 1333−1346.
(12) Niu, J.; Wang, B.; Feng, C.; Chen, K. Experimental Research on Viscosity Characteristics of Grouting Slurry in a High Ground Temperature Environment. *Materials* **2020**, *13*, 3221.
(13) Vidal, A.-V.; Araujo, R.-G.-S.; Freitas, J.-C.-O. Sustainable cement slurry using rice husk ash for high temperature oil well. *J. Clean. Prod.* **2018**, *204*, 292−297.
(14) Damion, T.; Chaunsali, P. Evaluating acid resistance of Portland cement, calcium aluminate cement, and calcium sulfoaluminate based cement using acid neutralization. *Cem. Concr. Res.* **2022**, *162*, No. 107000.
(15) Mo, L.; Deng, M.; Liu, K.; Tang, J. Deterioration mechanism of Portland cement paste subjected to sodium sulfate attack. *Adv. Cem. Res.* **2015**, *27*, 477−486.
(16) Chen, J.; Bharata, R.; Yin, T.; Wang, Q.; Wang, H.; Zhang, T. Assessment of sulfate attack and freeze−thaw cycle damage of cement-based materials by a nonlinear acoustic technique. *Mater. Struct.* **2017**, *50*, 105.
(17) Feng, P.; Garboczi, E.-J.; Miao, C.-W.; Bullard, J.-W. Microstructural origins of cement paste degradation by external sulfate attack. *Constr. Build. Mater.* **2015**, *96*, 391−403.
(18) Zhang, T.; Ma, B.-G.; Tan, H.-B.; Qi, H.-H.; Shi, T. Effect of sodium carbonate and sodium phosphate on hydration of cement paste. *J. Build. Eng.* **2022**, *45*, No. 103577.
(19) Yin, S. h.; Yang, Y. f.; Zhang, T. s.; Guo, G. f.; Yu, F. Effect of carbonic acid water on the degradation of Portland cement paste: Corrosion process and kinetics. *Constr. Build. Mater.* **2015**, *91*, 39−46.
(20) Xue, W.-P.; Liu, X.-Y.; Jing, W.; Yao, Z.-S.; Gao, C.; Li, H.-P. Experimental study and mechanism analysis of permeability sensitivity of mechanically damaged concrete to confining pressure. *Cem. Concr. Res.* **2020**, *134*, No. 106073.
(21) Li, L.-Y.; Easterbrook, D.; Xia, J.; Jin, W.-L. Numerical simulation of chloride penetration in concrete in rapid chloride migration tests. *Cement. Concrete. Comp.* **2015**, *63*, 113−121.
(22) Hong, Z.-J.; Zuo, J.-P.; Liu, C.; Zhang, Z.-S. Hydration and microstructure of nano-clay cement material in ion erosion solution. *Mater. Lett.* **2019**, *252*, 27−30.
(23) Wang, Y.; An, M. z.; Yu, Z. r.; Han, S.; Ji, W. y. Durability of reactive powder concrete under chloride-salt freeze−thaw cycling. *Mater. Struct.* **2017**, *50*, 18.
(24) Wang, Y.-Y.; Zhao, L.-H.; Zhao, J. Effects of Submicron Metakaolin on Hydration and Compressive Strength of Portland Cement Slurry. *Ksce. J. Civ. Eng.* **2021**, *25*, 2631−2639.
(25) Feng, B.-W.; Liu, J.-S. Durability of repair metakaolin geopolymeric cement under different factors. *Processes.* **2022**, *10*, 1818.
(26) Xu, O.-M.; Yang, X.-H.; Xiang, S.-L.; Zhang, H. Migration characteristic and model of chloride ions for NaCl-based salt storage asphalt mixtures. *Constr. Build. Mater.* **2021**, *280*, No. 122482.
(27) Lothenbach, B.; Winnefeld, F.; Alder, C.; Wieland, E.; Lunk, P. Effect of temperature on the pore solution, microstructure and hydration products of Portland cement pastes. *Cem. Concr. Res.* **2007**, *37*, 483−491.
(28) Gbozee, M.; Zheng, K.; He, F.-Q.; Zeng, X.-H. The influence of aluminum from metakaolin on chemical binding of chloride ions in hydrated cement pastes. *Appl. Clay. Sci.* **2018**, *158*, 186−194.
(29) Demir, İ.; Güzelkücük, S.; Sevim, Ö. Effects of sulfate on cement mortar with hybrid pozzolan substitution. *Eng. Sci. Technol. Int. J.* **2018**, *21*, 275−283.
(30) Lin, F.; Meyer, C. Hydration kinetics modeling of Portland cement considering the effects of curing temperature and applied pressure. *Cem. Concr. Res.* **2009**, *39*, 255−265.
(31) Yu, C.; Sun, W.; Scrivener, K. Mechanism of expansion of mortars immersed in sodium sulfate solutions. *Cem. Concr. Res.* **2013**, *43*, 105−111.
(32) Fan, Y.-F.; Luan, H.-Y. Pore structure in concrete exposed to acid deposit. *Constr. Build. Mater.* **2013**, *49*, 407−416.

https://doi.org/10.1021/acsomega.4c04434
ACS Omega 2024, 9, 44251−44261